Journal of Solid State Chemistry 184 (2011) 2398–2404

Contents lists available at ScienceDirect

Journal of Solid State Chemistry

journal homepage: www.elsevier.com/locate/jssc

A new ordered triple Hollandite: $Ba_{1.33}Sb_{2.66}Al_{5.33}O_{16}$

A. Letrouit, S. Boudin*, N. Barrier, R. Retoux

Laboratoire CRISMAT UMR6508, ENSICAEN, Université de Caen-Basse Normandie, 6 Bd Maréchal Juin, 14050 Caen Cedex, France

ARTICLE INFO

Article history:
Received 11 April 2011
Received in revised form
7 July 2011
Accepted 10 July 2011
Available online 23 July 2011

Keywords:
Hollandite
Powder diffraction
Electron microscopy
Li-ion cell

ABSTRACT

$Ba_{1.33}Sb_{2.66}Al_{5.33}O_{16}$ is a triple Hollandite, which crystallizes in a tetragonal cell ($I4/m$ no. 87) with $a=b=9.86090(5)$ Å and $c=8.77612(6)$ Å. Its crystal structure was characterized using electron diffraction and X-ray powder diffraction; it is isotypic to $K_{1.33}Mg_{3.11}Sb_{4.89}O_{16}$, $K_{1.76}Mg_{3.25}Sb_{4.75}O_{16}$ and to $K_{1.8}Li_{2.45}Sb_{5.55}O_{16}$. In the rutile chains of $Ba_{1.33}Sb_{2.66}Al_{5.33}O_{16}$, the ordering of Al and Sb atoms into unmixed sites induces the tripling of the c parameter compared to a 'single' Hollandite structure. The Ba^{2+} cations are dispersed along c, in the largest tunnels on non-split and fully occupied sites. They lie into Ba–Ba pairs separated by vacancies. Their regular arrangement has been confirmed by high resolution electron microscopy. Electrochemical experiments have also been performed in Li-ion cell but no Li insertion was detected.

1. Introduction

Hollandite-type compounds can be described by the general chemical formula $A_{2-x}M_8X_{16}$ (A=Ba, Pb, K, Rb, Cs, etc.; M=Mn, Ti, Al, Cr, Mo, Ga, etc.; X=O and OH^-), where A is a large cation located in the widest tunnels, M is a medium cation exhibiting an octahedral coordination. These compounds have been studied for numerous applications as, for example, one-dimensional ionic conductors of alkali ions [1], nuclear waste immobilizers [2], ions insertion/extraction [3], NO_x reduction catalysts [4] or photocatalysts [5].

Antimony oxides exhibit interesting properties such as ionic conduction [6] or lithium insertion/deinsertion [7–9], however few antimony Hollandite have been reported (see for example Refs. [10–13]). In order to isolate new antimony Hollandites, we decided to investigate the Ba^{2+}–Sb^{x+}–Al^{3+}–O^{2-} system (with $3 \leq x \leq 5$). In the expected materials the dispersion of the post-transition metallic Sb^{x+} ions into an inert barium aluminate matrix is susceptible to promote through amorphisation Li insertion/deinsertion properties, as observed in tin oxides composites [14]. Within the A^{2+}–Sb^{x+}–Al^{3+}–O^{2-} system (with A=earth alkaline) only few compounds have been reported [15–17], all of them exhibiting a layered structure.

We present here the new $Ba_{1.33}Sb_{2.66}Al_{5.33}O_{16}$ Hollandite. Its synthesis and its structure characterization based on electron diffraction (ED), X-ray powder diffraction (XRPD) and high resolution electron microscopy (HREM) are detailed. Electrochemical experiments of Li insertion/deinsertion are also presented.

2. Experimental

2.1. Synthesis

The $Ba_{1.33}Sb^{+5}_{2.66}Al_{5.33}O_{16}$ phase was isolated in a sample with the $BaSb^{+4}_{5.5}Al_{3.5}O_{17.25}$ nominal composition. Its solid state synthesis was performed in two steps. First $BaCO_3$ and Al_2O_3 were mixed in the 1:1.75 ratio. The mixture was placed in a platinum crucible and heated in air at 1000 °C for decarbonatation. Secondly Sb_2O_3 and Sb_2O_5 were added in equal proportion in order to lead to $BaSb^{+4}_{5.5}Al_{3.5}O_{17.25}$ (nominal composition). The sample, placed in alumina tube and sealed in evacuated quartz ampoule, was heated at 1000 °C for 12 h, cooled down to 700 °C for 50 h and quenched to room temperature. According to XRPD analyses (Fig. 1), a mixture of $Ba_{1.33}Sb^{+5}_{2.66}Al_{5.33}O_{16}$ and $BaSb^{+5}_2O_6$ (PDF#: 01–082-0520) was observed inside the alumina tube and Sb_2O_3 was found on the inner wall of the quartz ampoule. Attempts to synthesize monophasic samples of $Ba_{1.33}Sb^{+5}_{2.66}Al_{5.33}O_{16}$, using only $BaCO_3$, Sb_2O_5 and Al_2O_3 precursors in the 1.33:1.33:2.66 ratio, failed and led to a mixture of $BaSb^{+5}_2O_6$, $AlSb^{+5}O_4$ (PDF#: 01–074-6326) and unidentified phases without $Ba_{1.33}Sb^{+5}_{2.66}Al_{5.33}O_{16}$. Such experiments clearly indicate that an excess of Sb_2O_3 is necessary to synthesize $Ba_{1.33}Sb_{2.66}Al_{5.33}O_{16}$ in an evacuated ampoule. It is due to the fact that Sb_2O_5 can decompose into O_2 and volatile Sb_2O_3 oxide and an initial excess of Sb_2O_3 allows the stabilization of Sb_2O_5 and then its reaction with other precursors. The following studies, presented in this paper, have been performed using the $Ba_{1.33}Sb_{2.66}Al_{5.33}O_{16}$ and $BaSb_2O_6$ mixture extracted from the alumina tube.

2.2. Electron microscopy

Transmission electron microscopy samples were prepared by crushing the powder sample in butanol. The flakes in suspension

* Corresponding author. Fax: +33 2 31 95 16 00.
E-mail address: sophie.boudin@ensicaen.fr (S. Boudin).

0022-4596/$ - see front matter © 2011 Elsevier Inc. All rights reserved.
doi:10.1016/j.jssc.2011.07.010

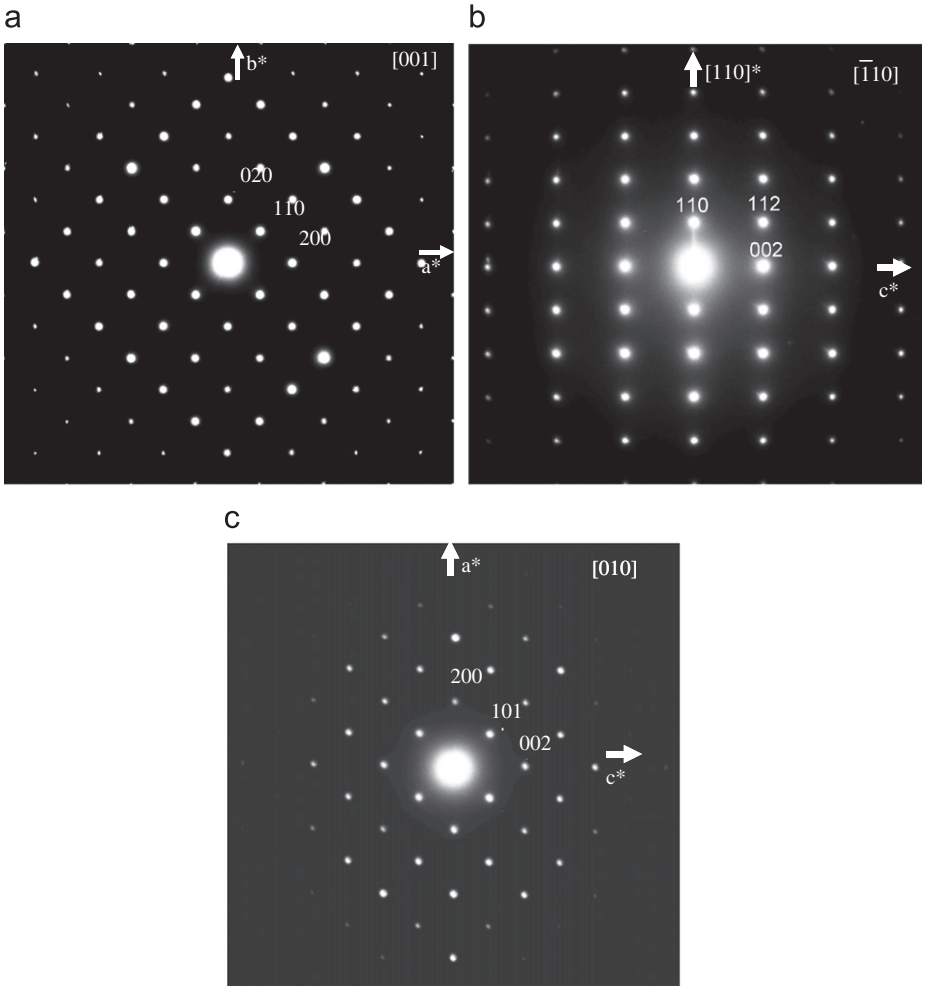

Fig. 1. [0 0 1] (a), [1̄ 1 0] (b), and [0 1 0] (c) electron diffraction patterns of $Ba_{1.33}Sb_{2.66}Al_{5.33}O_{16}$.

were deposited onto a holey carbon film, supported by a copper grid. Electron diffraction (ED) experiments were carried out using JEOL 2010 electron microscope (200 kV, tilt $\pm 60^{\circ}$). The high resolution electron microscopy (HREM) studies were performed using a FEI TECNAI G^2 30UT (300 kV, Cs = 0.65 mm, tilt $\pm 25^{\circ}$) and a JEOL 2010 FEG, (200 kV, Cs = 1.4 mm, tilt $\pm 42^{\circ}$) fitted with double tilt sample holders. Both microscopes are equipped with EDAX energy dispersive spectroscopy (EDS) analyzers. Theoretical images were calculated using Mac Tempas software, for different focus and crystal thickness values, combining the structural parameters deduced from X-ray powder diffraction (XRPD) study and the microscopes characteristics.

2.3. X-ray powder diffraction

X-ray diffraction measurement was performed using a Bruker D8 diffractometer with pure copper Cu $K_{\alpha 1}$ radiation ($\lambda =$ 1.54060 Å), selected by an incident germanium monochromator and equipped with a Lynx-Eye detector. The data were collected for 2θ varying from 10° to 120° for 5 s per 0.0092° step. The Rietveld refinement was performed with the Fullprof suite softwares [18].

2.4. Cyclic voltammetry

Electrochemical Li insertion/deinsertion in $Ba_{1.33}Sb_{2.66}Al_{5.33}O_{16}$ was tested using a Swagelok®-type cell with a Li anode and a cathode composed of a mixture $Ba_{1.33}Sb_{2.66}Al_{5.33}O_{16}$ (87%)/$BaSb_2O_6$ (13%) (in molecular ratios). The positive electrode was prepared from a mixture of $Ba_{1.33}Sb_{2.66}Al_{5.33}O_{16}$/$BaSb_2O_6$, carbon black (Superior Graphite) and binder (PVDF) dissolved in NMP (N-Methyl-2-Pyrrolidone) in weight ratios 75%/15%/10%. The resulting slurry was spread onto a copper foil, dried in oven at 70 °C for 1 h, cut into disks of 12 mm diameter and pressed. The cell was assembled in an Ar filled glovebox (with less than 1 ppm of O_2 and H_2O). It is composed of a Li counter electrode, a 1 M solution of $LiPF_6$ dissolved in ethylene carbonate/diethyl carbonate electrolyte (EC:DEC 2:1 in volume) used as the electrolyte and the previous positive electrode. The charge–discharge cycling of the cell was performed at room temperature using a potentiostat–galvanostat VMP2 (Biologic). Similar cells with only superior carbon and binder as positive electrode were fabricated in order to compare the electrochemical activities of both cells.

3. Structural determination

3.1. Energy dispersive spectroscopy (EDS) analysis and electron diffraction (ED)

EDS analyses performed on numerous crystallites of $Ba_{1.33}Sb_{2.66}Al_{5.33}O_{16}$ demonstrated a homogeneous composition and led to the averaged cationic ratios: Ba/Sb/Al = 13%/27%/60%, in accord with the 14%/28%/56% ratios deduced from the chemical formula.

The reconstruction of the reciprocal lattice was carried out on numerous $Ba_{1.33}Sb_{2.66}Al_{5.33}O_{16}$ crystallites by tilting around the crystallographic axes. This ED study shows that the crystallites

present a tetragonal structure with cell parameters close to $a \approx 9.9$ Å and $c \approx 8.8$ Å and with the systematic ($h+k+l=2n$) existence conditions on all ED patterns. Here only the basic [0 0 1], [$\bar{1}$ 1 0] and [0 1 0] ED patterns of $Ba_{1.33}Sb_{2.66}Al_{5.33}O_{16}$ are given in Fig. 1a–c, respectively. The existence conditions ($h+k+l=2n$) are compatible with the tetragonal space groups $I4$ (no. 79), $I\bar{4}$ (no. 82), $I4/m$ (no. 87), $I422$ (no. 97), $I4mm$ (no. 107), $I\bar{4}2m$ (no. 121), $I4/mmm$ (no. 139).

3.2. X-ray powder diffraction (XRPD)

The cell parameters and the possible space groups deduced from the ED study suggest that the $Ba_{1.33}Sb_{2.66}Al_{5.33}O_{16}$ phase is isotypic to the $K_xMg_{(8+x)/3}Sb_{(16-x)/3}O_{16}$ triple Hollandite [13], which crystallizes in the $I4/m$ space group with $a=10{,}3256(6)$ Å and $c=9{,}2526(17)$ Å. Consequently, after the cell and profile parameters refinement, the Sb, Al and O atoms were placed using the atomic coordinates of the Sb/Mg and O sites, respectively, of the $K_xMg_{(8+x)/3}Sb_{(16-x)/3}O_{16}$ phase. Initially the cationic sites of the rutile chains (labelled M1 and M2 in $K_xMg_{(8+x)/3}Sb_{(16-x)/3}O_{16}$) were considered with an occupation of 33%/66% for Sb/Al, in agreement with the EDS analysis. Subsequently, occupations of the $M1$ and $M2$ sites were refined and were finally fixed to a full Sb occupation for $M1$ and to a full Al occupation for $M2$. The Ba site was located using different Fourier maps; a single crystallographic site with a full occupation was found for this atom whereas several partially occupied sites were found for K atoms in $K_xMg_{(8+x)/3}Sb_{(16-x)/3}O_{16}$.

In the final Rietveld refinement, $Ba_{1.33}Sb_{2.66}Al_{5.33}O_{16}$ and the impurity $BaSb_2O_6$ were taken into account. The profile and cell parameters, the atomic coordinates and the Sb and Ba isotropic atomic displacement parameters were adjusted for $Ba_{1.33}Sb_{2.66}Al_{5.33}O_{16}$, the profile and cell parameters and the atomic coordinates were adjusted for $BaSb_2O_6$. According to the Rietveld refinement, the molecular ratios of the $Ba_{1.33}Sb_{2.66}Al_{5.33}O_{16}$/$BaSb_2O_6$ mixture are 87%/13%, respectively. The experimental, calculated and different diffractograms are reported in Fig. 2. The pertinent parameters for the X-ray recordings and for the refinement are reported in Table 1. The atomic parameters of $Ba_{1.33}Sb_{2.66}Al_{5.33}O_{16}$ are reported in Table 2. The distances and angles are reported in Table 3.

Table 1
Pertinent parameters for data collection and refinement for $Ba_{1.33}Sb_{2.66}Al_{5.33}O_{16}$.

Data collection	
Diffractometer	D8 Advance Vario1 Brüker
Radiation	1.54060 Å (Cu $K\alpha_1$, germanium monochromator)
2θ range (deg.)	10–120
Step	0.0092
Counting time/point	5 s
Refinement parameters for $Ba_{1.33}Sb_{2.66}Al_{5.33}O_{16}$	
Space group	$I4/m$ (no. 87)
cell parameters	$a=b=9.86090(5)$ Å $c=8.77612(6)$ Å $\alpha=\beta=\gamma=90^\circ$ $V=853.367(8)$ Å^3
Number of reflections	343
Number of refined parameters (global and impurity phase parameters excluded)	27
Profile function	Thompson-Cox—Hastings pseudo-Voigt
Half width parameters (U, V, W, Y, SZ)	0.0441(3), −0.0266(2), 0.01207(7), 0.05210(7), −0.552(1)
Anisotropic Lorentzian size broadening	Applied to $hk0$ reflections
Preferred orientation correction, direction and parameters	March–Dollase model, 00l, $G1=1.02812(3)$.
R_{Bragg}	8.00%
R_F	5.49%
Other refinement parameters	
Background correction	Polynomial function
R_p	11.6%
R_{wp}	15.5%
R_{exp}	7.58%
ρ_{max}; ρ_{min}(e/Å^3)	2.39; −1.23
Molecular ratios of $Ba_{1.33}Sb_{2.66}Al_{5.33}O_{16}$/$BaSb_2O_6$ in powder samples	87%/13%

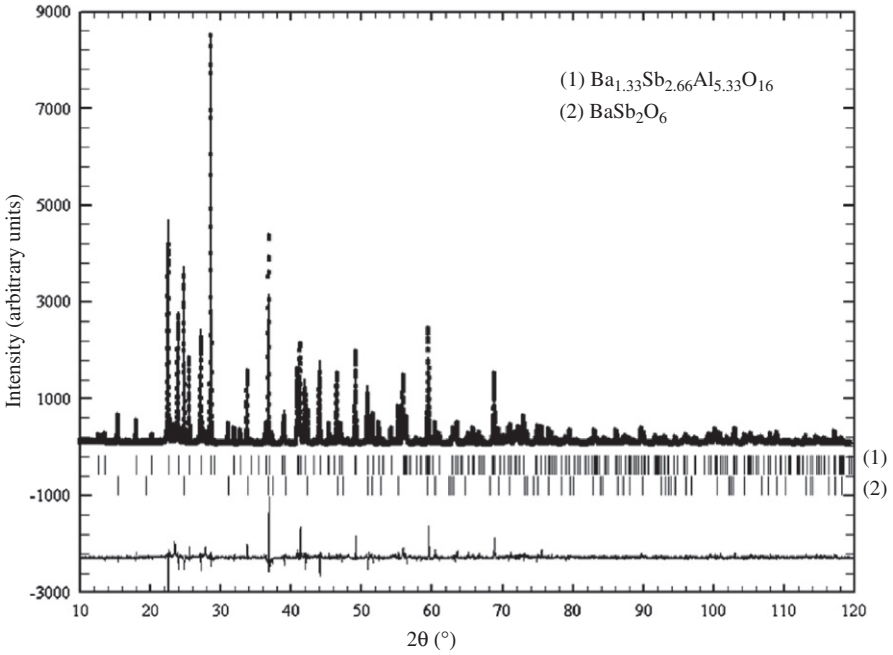

Fig. 2. Experimental (solid dot), calculated (upper solid line) and difference (lower solid line) XRPD patterns of $Ba_{1.33}Sb_{2.66}Al_{5.33}O_{16}$. The vertical bars indicate the positions of the Bragg reflections of $Ba_{1.33}Sb_{2.66}Al_{5.33}O_{16}$ and $BaSb_2O_6$ (upper and lower, respectively).

Table 2
Atomic parameters for $Ba_{1.33}Sb_{2.66}Al_{5.33}O_{16}$.

Atom	Site	x	y	z	B_{iso} (Å^2)	Site occupation (%)
Sb	8*h*	0.3509(2)	0.1640(2)	0.00000	0.10(3)	100
Ba	4*e*	0.00000	0.00000	0.2114(3)	1.31(6)	100
Al	16*i*	0.3488(6)	0.1649(6)	0.3350(5)	0.50[a]	100
O(1)	8*h*	0.152(2)	0.205(1)	0.00000	1.00[a]	100
O(2)	16*i*	0.156(1)	0.197(1)	0.330(1)	1.00[a]	100
O(3)	8*h*	0.550(1)	0.164(2)	0.00000	1.00[a]	100
O(4)	16*i*	0.536(1)	0.1677(9)	0.330(1)	1.00[a]	100

[a] Fixed parameters.

Table 3
Distances (Å) and angles (deg.) in $Ba_{1.33}Sb_{2.66}Al_{5.33}O_{16}$.

Distances (Å)		Angles (deg.)	
Sb–O(1)	2.00(2)	O(1)–Sb–O(2)	80.3 (8) × 2
Sb–O(2)	2.02(1) × 2	O(1)–Sb–O(3)	168 (1)
Sb–O(3)	1.96(1)	O(1)–Sb–O(4)	92.3 (8) × 2
Sb–O(4)	1.97(1) × 2	O(2)–Sb–O(2)	94.9 (7)
Average	1.99(1)	O(2)–Sb–O(3)	91.7 (8) × 2
		O(2)–Sb–O(4)	82.6 (6) × 2/172.5 (9) × 2
Al–O(1)	1.93(1)	O(3)–Sb–O(4)	95.4 (9) × 2
Al–O(2)	1.93 (1)/1.99(1)	O(4)–Sb–O(4)	99.0 (8)
Al–O(3)	1.84(1)		
Al–O(4)	1.85 (1)/1.93(1)	O(1)–Al–O(2)	84.3(8)/95.4 (6)
Average	1.91(1)	O(1)–Al–O(3)	79.5 (9)
		O(1)–Al–O(4)	90.9 (8)/174.8 (9)
Ba–O(1)	3.13(1) × 4	O(2)–Al–O(2)	81.3 (7)
Ba–O(2)	2.69(1) × 4	O(2)–Al–O(3)	92.8 (8)/172.6 (9)
Ba–O(4)	3.315(10) × 4	O(2)–Al–O(4)	84.4 (7)/89.6 (8)/90.5 (8)/169 (1)
		O(3)–Al–O(4)	95.7 (8)/100.2 (7)
		O(4)–Al–O(4)	94.3 (8)

4. Results and discussion

4.1. Structural description

$Ba_{1.33}Sb_{2.66}Al_{5.33}O_{16}$ Hollandite structure is built up from double ribbons of edge-sharing SbO_6 and AlO_6 octahedra (ie. double rutile chains), running along *c* (Figs. 3 and 4). The antimono–aluminate framework exhibits two types of tunnels directed along *c* and labelled A and B. The A tunnels are delimited by four double ribbons and contain the Ba^{2+} cations, while the B tunnels are delimited by four single ribbons and are empty.

In a 'simple' Hollandite with cell parameters equal to $a \approx 10$ Å and $c \approx 2.9$ Å, the cationic sites within the tunnels are close to each other and only distant to 2.8–2.9 Å. In non-fully occupied Hollandites, partial occupations and split sites can be observed in order to minimize the cation–cation repulsions. Such arrangements can lead to super or modulated structures [19–21]. $Ba_{1.33}Sb_{2.66}Al_{5.33}O_{16}$ is a triple Hollandite, with the *c* parameter tripled compared to a 'simple' Hollandite. It is isotypic to the $K_{1.33}Mg_{3.11}Sb_{4.89}O_{16}$, $K_{1.76}Mg_{3.25}Sb_{4.75}O_{16}$ and $K_{1.8}Li_{2.45}Sb_{5.55}O_{16}$ antimony Hollandites. The *a* and *c* cell parameters of $Ba_{1.33}Sb_{2.66}Al_{5.33}O_{16}$ are shorter than those of potassium antimony Hollandites, in agreement with the smaller sizes of the cations $((1.33/2)r(Ba^{2+}) \approx (1.33/2)r(K^+) < (1.76/2)r(K^+) \approx (1.8/2)r(K^+)$ and $(2.66r(Sb^{5+})+5.33r(Al^{3+}))/8 < (3.11r(Mg^{2+})+4.89r(Sb^{5+}))/8 \approx (3.25r(Mg^{2+})+4.75r(Sb^{5+}))/8 \approx (2.45r(Li^+)+5.55r(Sb^{5+}))/8)$. In the latter triple Hollandites, the superstructure is due systematically to an ordering of K^+ and Ba^{2+} cations within the large tunnels and possibly to an ordering of the Sb^{5+} cations within the rutile chains.

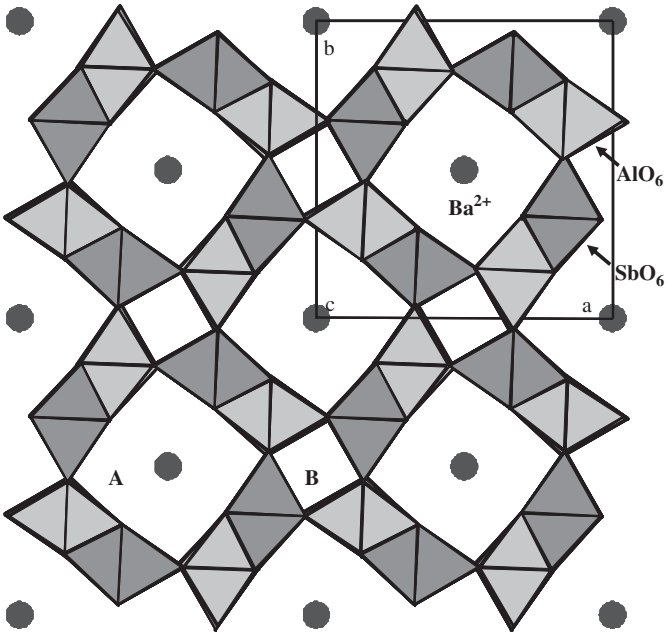

Fig. 3. Structure of $Ba_{1.33}Sb_{2.66}Al_{5.33}O_{16}$ projected along the *c*-axis. The SbO_6 and AlO_6 polyhedra are represented in dark and light grey, respectively. Spheres are Ba ions.

In $K_{1.76}Mg_{3.25}Sb_{4.75}O_{16}$ and $K_{1.8}Li_{2.45}Sb_{5.55}O_{16}$, which have been studied by single crystal X-ray diffraction, three cationic cavities lie over one *c* cell range as shown in Fig. 5; they correspond to two different crystallographic sites, labelled C1 and C2 by Michiue [13]. Such sites alternate along one tunnel into the sequence …C1–C2–C1–C1–C2–C1…. In $K_{1.76}Mg_{3.25}Sb_{4.75}O_{16}$ the C1 site, occupied at 82%, is split into three sites *K*1, *K*3 and *K*5 whereas the C2 site, fully occupied, is split into two sites *K*2 and *K*4. In $K_{1.8}Li_{2.45}Sb_{5.55}O_{16}$ the C1 site, occupied at 87%, is split into two sites *K*2 and *K*3 whereas the C2 sites, occupied at 96%, is split into two sites *K*1 and *K*4. For $K_{1.33}Mg_{3.11}Sb_{4.89}O_{16}$, a cationic distribution along the tunnels has been proposed based on High Resolution Electron Microscopy (HREM) study and images simulations. The K^+ cations are located on sites equivalent to C1 centres with a full occupancy, as result along the tunnels K^+–K^+ pairs are separated by C2 vacancies. In $Ba_{1.33}Sb_{2.66}Al_{5.33}O_{16}$ only the C1 cavity is occupied with one non-split and fully occupied site contrary to $K_{1.76}Mg_{3.25}Sb_{4.75}O_{16}$ and $K_{1.8}Li_{2.45}Sb_{5.55}O_{16}$ and similarly to $K_{1.33}Mg_{3.11}Sb_{4.89}O_{16}$. In the $K_{1.33}Mg_{3.11}Sb_{4.89}O_{16}$ HREM model, the *K* site was located at the centre of the C1 cavity and could not be adjusted. In $Ba_{1.33}Sb_{2.66}Al_{5.33}O_{16}$, the refined Ba site was found shifted away from the centre of the C1 cavity and directed toward the C2 cavity. In such arrangement, the Ba^{2+}–Ba^{2+} repulsions are minimized with Ba–Ba distances alternatively equal to 3.711(5) Å and 5.066(5) Å. Difference Fourier maps exhibit main electronic residues (with $2.15\ e/Å^3 < \rho < 2.40\ e/Å^3$) on Sb atoms and weaker residues (with $\rho < 2.15\ e/Å^3$) along the tunnels around the Ba site and at the centre of the C2 cavity. Attempts to split the Ba atom around the Ba site and on the weak residues sites led to higher agreement factors, confirming one single crystallographic site for Ba. The Ba atoms, off centred inside the C1 cavities, exhibit a distorted cuboctahedral coordination with 4 short, 4 intermediate and 4 long Ba–O distances (equal to 2.69(1), 3.13(1) and 3.315 (10) Å, respectively).

In $K_{1.33}Mg_{3.11}Sb_{4.89}O_{16}$ and $K_{1.8}Li_{2.45}Sb_{5.55}O_{16}$, the two crystallographic metallic sites (*M*1 and *M*2) of the rutile chain have been proposed with equivalent mixed occupancies. Thus no ordering within the rutile chains was retained and the tripling of the *c* parameter is only due to the ordering of the K cations within the

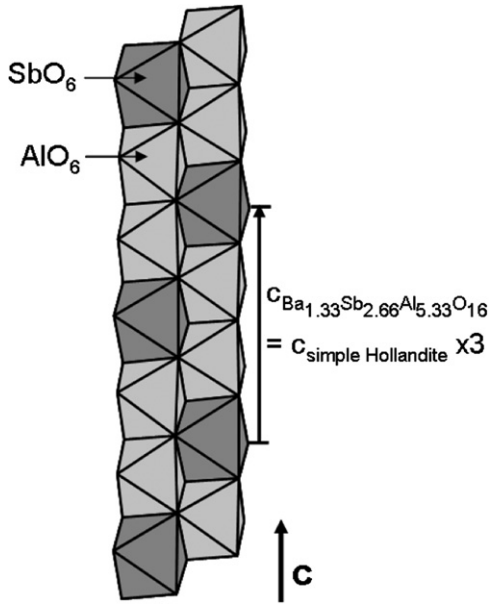

Fig. 4. Double rutile chains in $Ba_{1.33}Sb_{2.66}Al_{5.33}O_{16}$. The SbO_6 and AlO_6 polyhedra are represented in dark and light grey, respectively.

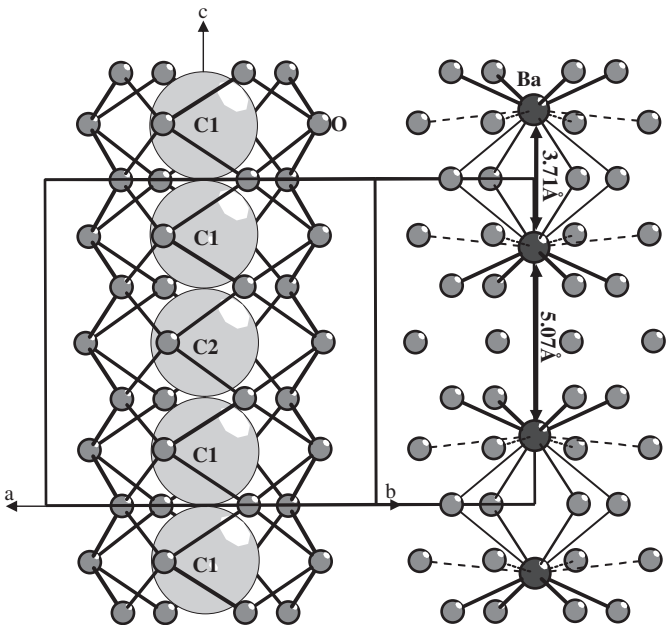

Fig. 5. Disposition of C1 and C2 cavities (left) and Ba^{2+} ions (right) inside the A tunnels of $Ba_{1.33}Sb_{2.66}Al_{5.33}O_{16}$. Ba,O and cavities are represented with black, grey and light grey balls. Short, intermediate, long Ba–O distances are represented with bold, normal and dash sticks (right).

tunnels. For $K_{1.76}Mg_{3.25}Sb_{4.75}O_{16}$, two Mg/Sb mixed metallic sites with different occupancies were found. Along a rutile chain one $Mg_{0.898}Sb_{0.102}$ site (*M*1 site) alternates with two $Mg_{0.161}Sb_{0.839}$ sites (*M*2 sites). For this Hollandite, the tripling of the cell results simultaneously from K and Mg/Sb orderings. In $Ba_{1.33}Sb_{2.66}Al_{5.33}O_{16}$, one unmixed Sb site alternates with two unmixed *Al* sites in a rutile chain, as shown in Fig. 4. The SbO_6 octahedron is slightly distorted with Sb–O distances ranging from 1.97(1) to 2.02(1) Å and O–Sb–O right angles ranging from 80.3(8)° to 99.0(8)° (Table 3). The AlO_6 octahedron is more distorted with Al–O distances ranging from 1.84(1) to 1.99(1) Å and O–Al–O right angles ranging from 79.5(9)° to 100.2(7)° (Table 3). Contrary to $K_{1.33}Mg_{3.11}Sb_{4.89}O_{16}$ and $K_{1.8}Li_{2.45}Sb_{5.55}O_{16}$ and similarly to $K_{1.76}Mg_{3.25}Sb_{4.75}O_{16}$, the $Ba_{1.33}Sb_{2.66}Al_{5.33}O_{16}$ Hollandite exhibits an ordering of the Sb cations within the rutile chains. In $Ba_{1.33}Sb_{2.66}Al_{5.33}O_{16}$, the Sb and Al cations are 'fully' ordered without the presence of Sb/Al mixed sites.

4.2. High resolution electron microscopy (HREM) study

We have reported here the most characteristic contrasts of the HREM images recorded on two different crystallographic orientations [0 0 1] and [$\bar{1}$ 1 0]. The theoretical images calculation were performed through focus series and are inserted in the figures.

Most typical [0 0 1] contrasts of HREM observations of $Ba_{1.33}Sb_{2.66}Al_{5.33}O_{16}$ are presented in Fig. 6a and b. Fig. 6a is recorded

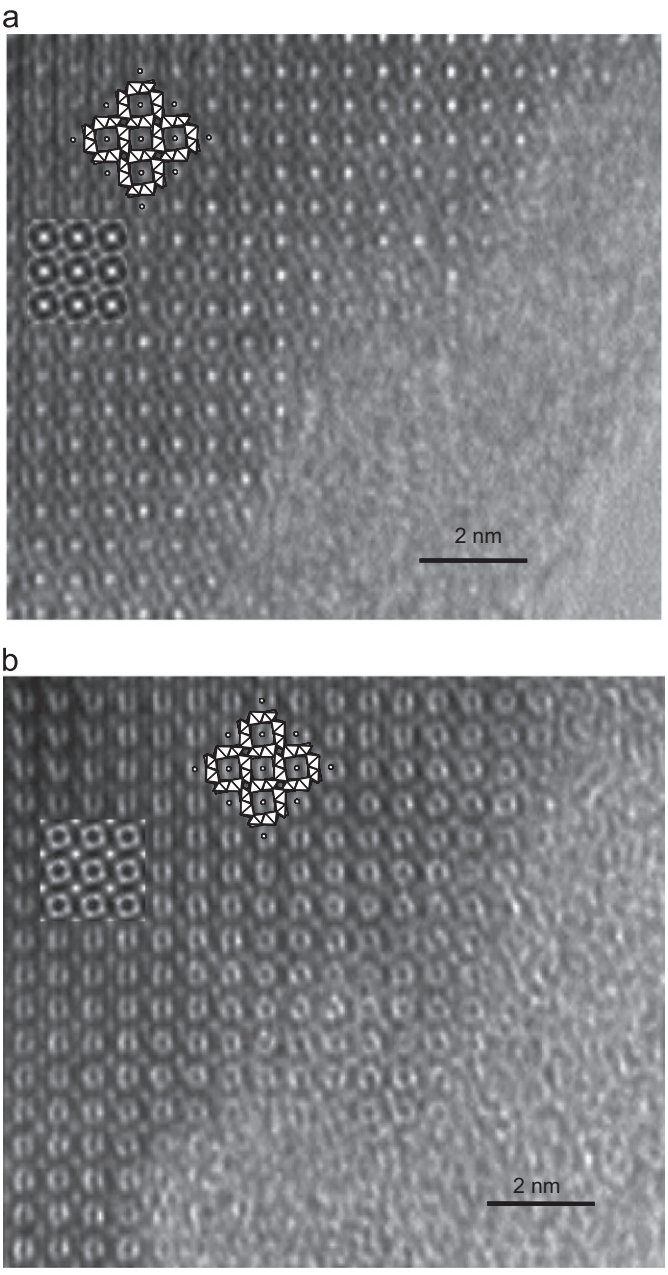

Fig. 6. (a) [0 0 1] Experimental and calculated (in inset) high resolution electron microscopy images for a focus value close to −760 Å (thickness: 30 Å). (b) [0 0 1] Experimental and calculated (in inset) high resolution electron microscopy images for a focus value close to −400 Å (thickness: 30 Å). On both images (upper part), the drawing of the structure projected along *c*-axis has been superimposed on the experimental image.

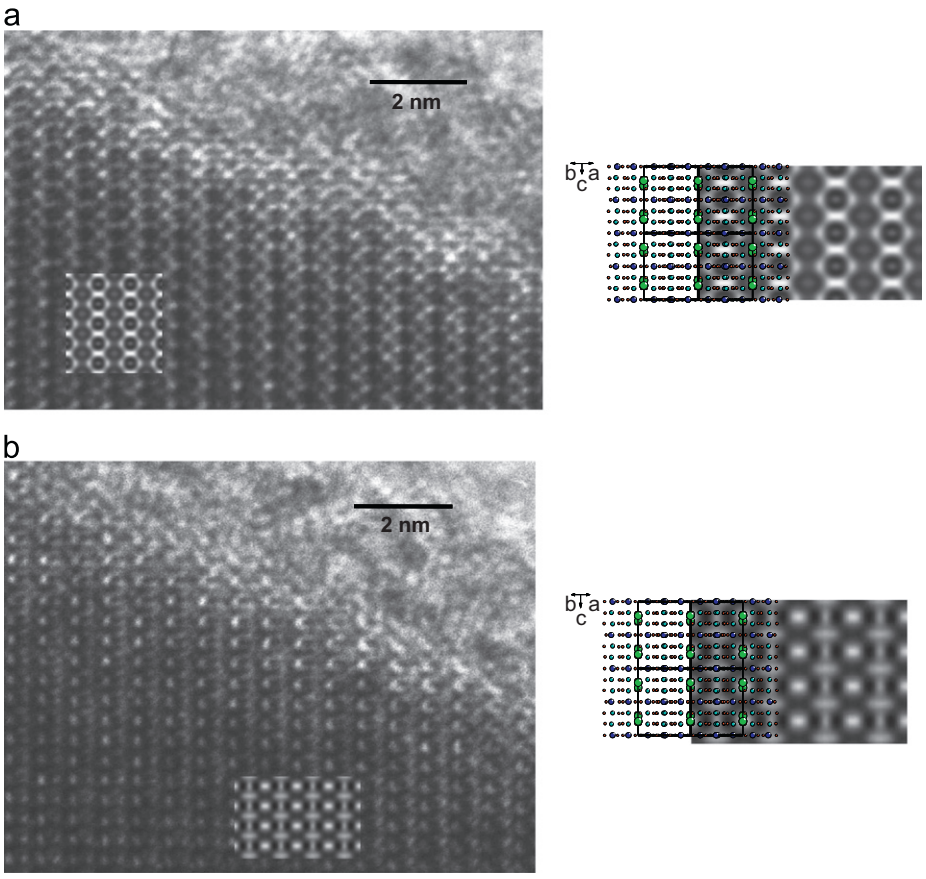

Fig. 7. (a) [$\bar{1}$ 1 0] Typical experimental and calculated (in inset) high resolution electron microscopy images for a focus value close to −250 Å (thickness: 30 Å). (b) [$\bar{1}$ 1 0] Typical experimental and calculated (in inset) high resolution electron microscopy images for a focus value close to −850 Å (thickness: 30 Å). On both images, for clarity, only the drawing of atomic stacking of the structure has been superimposed on the calculated HREM image (on the right part).

for a focus value close to −760 Å. It consists of a set of intense white dots surrounding successively by a black and white circle. The low electron densities are represented in black whereas the columns of Ba, Al and Sb atoms are in white. Here, the dark dots, located between four white circles, are representative of the small empty tunnels. Fig. 6b is recorded at a focus value close to the Scherzer (−400 Å), where high electron density zones appear more or less as dark contrasts. Here the opposite contrast compared to Fig. 6a is observed since dark intense dots are surrounded successively by white and black circles.

In order to comfort the Ba location in the A tunnels deduced from XRPD, we present here the High Resolution images recorded along [$\bar{1}$ 1 0]. Fig. 7a is recorded for a focus value close to −250 Å. Two types of lines are evidenced, one with a white dot at the centre surrounded successively by a black and a white circle and the second with a medium black dot surrounded by a black circle. The high electron densities are represented in white for Sb or Al atoms and in medium black for Ba atoms. Fig. 7b is recorded for a focus value close to −850 Å. It consists of two types of lines one with black and white dots and another with a vertically chain and horizontal dash. The Ba atoms are represented by white dots, Al atoms by vertically dash and Sb atoms by horizontal dash. The space between the white dots and the white dash corresponds to the low electron densities.

These [$\bar{1}$ 1 0] images (Fig. 7a and b) recorded perpendicularly to the tunnels are representative of the observations performed on large areas in the $Ba_{1.33}Sb_{2.66}Al_{5.33}O_{16}$ crystals. The stacking of the atoms is very regular and no defect can be evidenced in the $Ba_{1.33}Sb_{2.66}Al_{5.33}O_{16}$ crystals. According to the simulations based on XRPD, the Ba atoms are regularly stacked in the A tunnels and the Sb and Al atoms are not mixed on common sites, no modulation or variations of the contrasts are observed. These observations are in good agreement with electron diffraction studies. Indeed, we have not observed diffuse streaks on electron diffraction patterns. This confirms the differences between $Ba_{1.33}Sb_{2.66}Al_{5.33}O_{16}$ and the triple potassium antimony Hollandites in which the K cations are delocalized in the tunnels or the metallic cations sit on mixed sites in the rutile chains.

4.3. Li insertion/deinsertion properties

Hollandite-type structures have been extensively studied for lithium insertion/deinsertion properties [22–25] contrary to antimony oxides [7–9]. However, these latter compounds, like Sb_2O_3 and MSb_2O_6 (M=Ni,Co) exhibit interesting electrochemical activity towards lithium insertion/deinsertion. Based on these studies, we have undertaken electrochemical tests in a Li-ion cell where $Ba_{1.33}Sb_{2.66}Al_{5.33}O_{16}$ was used as the positive electrode. Cyclic voltammetry (CV) experiments were recorded between 0.01 and 2 V versus Li^+/Li at a rate of 1 mV/s. Similar experiments were performed in the same conditions for a cell with carbon black as the only active material in the positive electrode. As both voltammograms have quite identical shapes, the observed electrochemical activity cannot be attributed to the Hollandite phase. Consequently we concluded that $Ba_{1.33}Sb_{2.66}Al_{5.33}O_{16}$ exhibit no activity towards Li electrochemical insertion/deinsertion contrary to our expectations. This barium aluminate matrix apparently does not favour the antimony activity for insertion, and further investigations on other antimony oxides systems still need to be performed in order to understand the role of inert matrix in such materials.

5. Conclusion

The $Ba_{1.33}Sb_{2.66}Al_{5.33}O_{16}$ triple Hollandite has been isolated and characterized using electron diffraction, X-ray powder diffraction and high resolution electron microscopy. The antimono–aluminate framework is composed of rutile chains in which one Sb site alternates with two Al sites. The barium cations lie, in the largest tunnels, on one crystallographic site; no disorders have been observed along *c* neither by electron microscopy nor by X-ray diffraction. Despite the fact that up to 1/3 of the cationic sites is unoccupied in the largest tunnels, no activity was detected towards electrochemical Li insertion in $Ba_{1.33}Sb_{2.66}Al_{5.33}O_{16}$.

Additional information

Crystal structure of $Ba_{1.33}Sb_{2.66}Al_{5.33}O_{16}$ may be obtained from Fachinformationszentrum Karlsruhe data base at http://www.fiz-karlsruhe.de/request_for_deposited_data.html using the CSD-422875 reference.

Acknowledgments

We thank O. Crosnier and T. Brousse from Laboratoire de Génie des Matériaux et Procédés Associés of Polytech in Université de Nantes (France) for electrochemical study and for fruitfull discussions.

Appendix A. Supplementary materials

Supplementary materials associated with this article can be found in the online version at doi:10.1016/j.jssc.2011.07.010.

References

[1] S. Yoshikado, T. Ohachi, I Taniguchi, Y. Onoda, M. Watanabe, Y. Fujiki, Solid State Ionics 9–10 (1983) 1305.
[2] A.E. Ringwood, S.E. Kesson, N.G. Wate, W. Hibberson, A. Major, Nature 278 (1979) 219.
[3] Qi Feng, Hirofumi Kanoh, Yoshitaka Miyai, Kenta Ooi, Chem. Mater. 7 (1995) 148.
[4] T. Mori, S. Yamauchi, H. Yamamura, M. Watanabe, Appl. Catal., A 129 (1995) L1.
[5] T. Mori, J. Suzuki, K. Fujimoto, M. Watanabe, Y Hasegawa, Appl. Catal., B 23 (1999) 283.
[6] W.A. England, M.G. Cross, A. Hamnett, P.J. Wiseman, J.B. Goodenough, Solid State Ionics 1 (1980) 231.
[7] H Li, X. Huang, L. Chen, Solid State Ionics 123 (1999) 189–197.
[8] M.Z. Xue, Z.W. Fu, Electrochem. Commun. 8 (2006) 1250.
[9] D. Larcher, A.S. Prakash, L. Laffont, M. Womes, J.C. Jumas, J. Olivier-Fourcade, M.S. Hedge, J.M. Tarascon, J. Electrochem. Soc. 153 (9) (2006) A1778.
[10] G. Bayer, W. Hoffmann, Naturwissenschaften 53 (1966) 381.
[11] H. Watelet, J.P. Besse, G. Baud, R. Chevalier, Mater. Res. Bull. 17 (1982) 863–871.
[12] A. Pring, D.J. Smith, D.A. Jefferson, J. Solid State Chem. 46 (1983) 373.
[13] Y. Michiue, J. Solid State Chem. 3 (2007) 146.
[14] Y. Idota, T. Kubota, A. Matsufuji, Y. Maekawa, T. Miyasaka, Science 276 (1997) 1395.
[15] A. Letrouit, S. Boudin, R. Retoux, M. Hervieu, Solid State Sci. 10 (2008) 982–990.
[16] A. Letrouit, S. Boudin, R. Retoux, Solid State Sci. 11 (2009) 1183–1186.
[17] F. Emmerling, C. Reinhardt, S. Zimper, C. Roehr, Z. Naturforsch., B 60 (2005) 419.
[18] Fullprof Suite Program (1.00)—version February 2007, Carvajal J.R. (ILL, France), Roisnel T. (LCSIM, CNRS, France), Platas J.G. (ULL, Spain), Chapon L.C. (ISIS, RAL, UK).
[19] L.A. Bursill, G. Grzinic, Acta Crystallogr., B 63 (1980) 2902.
[20] S.B. Xiang, H.F. Fan, X.J. Wu, F.H. Li, Q. Pan, Acta Crystallogr., B 46 (1990) 929.
[21] H. Leligny, Ph. Labbé, M. Ledesert, B. Raveau, C. Valdez, W.H. McCaroll, Acta Crystallogr., B 48 (1992) 134.
[22] L.D. Noaills, C.S. Johnson, J.T Vaughey, M.M. Thackeray, J. Power Sources 81 (1999) 259–263.
[23] T. Matsumura, R. Kanno, Y. Inaba, Y. Kawamoto, M. Takano, J. Electrochem. Soc. 149 (2002) A1509–A1513.
[24] M. Sugantha, P.A. Ramakrishnan, A.M. Hermann, C.P. Warmsingh, D.S. Ginley, Int. J. Hydrogen Energy 28 (2003) 597–600.
[25] N. Sharma, J. Plévert, G.V. Subba Rao, B.V.R. Chowdari, T.J. White, Chem. Mater. 17 (2005) 4700–4710.